Development and validation in a 2D-GIS environment of a 3D shadow cast vector-based model on arbitrarily orientated and tilted surfaces

J.D. Viana-Fons[a], J. Gonzálvez-Maciá[a], J. Payá[a,*]

[a] Instituto Universitario de Investigación en Ingeniería Energética IUIIE, Universitat Politècnica de València
Camino de Vera s/n Ed 8E, Semisótano frente Acceso J., 46022 València, Spain

*Corresponding author. Tel.: +34 963879124; Fax: 34 963879126;
E-mail address: jorge.paya@iie.upv.es (J. Payá)

Abstract

This paper presents a systematic GIS-based methodology to obtain the shadow cast profile of a group of buildings on arbitrarily orientated and tilted surfaces. The model is integrated in the widely-employed 2D-GIS environment. Given its scalability, the methodology can be easily applied from a local level up to a district, city or even regional level. This work is of interest for a wide range of applications such as for instance in Solar Resource Assessments (SRA) in urban environments.

The starting point is to use cadastral cartography and LiDAR altimetric data to obtain a 3D vector-based model of the buildings using high robust mode estimators. Once the geometry of the buildings is defined, analytical models are applied to calculate the shadow cast profile on any arbitrarily orientated and tilted surface of the surroundings.

The model has been implemented in the R programming language. An extensive validation has been carried out for several buildings of Valencia (Spain) using CAD elevation views of the buildings and the SketchUp's shadow tool. The error of the vector-based city model is lower than 1% in all LiDAR datasets. The maximum error of the overall methodology, including both height and shadow models, is lower than 2%.

Keywords: urban shadow model, urban solar irradiation, 3D city model, daylight simulation, model validation, GIS

NOMENCLATURE

Symbols

Z	Height	XY	Ground coordinate
α	Plane azimuth or aspect	β	Plane elevation or slope
G	Centroid of a polygon	SF	Shadow factor
K	Kernel function	f	Probability density function
h	Bandwidth	λ	Power parameter of transformation
μ	Mean	σ	Standard deviation
B_0	Building footprint	B_h	Surface of interest projection onto π_h
B_n	Surface of interest on its plane	B_r	Surface of interest projection onto π_r
S_0	Shadow footprint	S_h	Shadow profile projection onto π_h
S_n	Shadow profile on its plane	S_r	Shadow profile projection onto π_r
p_0	Vertex of S_0	p_h	Vertex of S_h
p_n	Vertex of S_n	p_r	Vertex of S_r
π_h	Horizontal plane	π_n	Plane of the Surface of interest
π_r	Non-vertical rotated plane	$\hat{h}$	Direction vector of the π_h
$\hat{n}$	Direction vector of the π_n	$\hat{s}$	Direction vector of the sun
$\hat{u}$	Axis of rotation	θ	Angle of rotation

Estimators

EDFM	Empirical Probability Density Function mode		
HRM	Half-Range mode	HSM	Half-Sample mode
SM	Shorth mode	LMSM	Least Median of Squares mode
RPM	Robust Parametric mode	MAE	Mean Absolute Error
RMSE	Root-Mean-Square Error	RE	Relative Error

Abbreviations / subscripts

LiDAR	Light Detection and Ranging	LoD	Level of Detail
CAD	Computer-Aided Design	GIS	Geographic Information System
BIM	Building Information Modeling	DEM	Digital Elevation Model

1. Introduction

Urban areas currently concentrate around half of the world's population but consume over two-thirds of the world's energy and account for around the same share of CO_2 emissions [1]. This situation can be seen as an opportunity since cities could potentially cut their carbon emissions by 90 percent by 2050 [2] using current technologies and policies. This change in the paradigm of the cities has motivated the development and enrichment of 3D city models extending their functionality and usability in a perspective of sustainability [3]. Many of these applications are energy-related [4–6] and these 3D city models are the starting point in building or urban scales for assessing the urban solar resource [7]. In these applications, a correct shadow model is essential to make a suitable solar assessment, especially in urban contexts, where complex geometries cast very large and variable shadows resulting in a dramatic decrease of the incident solar radiation [8,9]. Accurate shadow models are essential in many research areas such as in urban daylight analysis, in urban building energy modelling or even for the analysis of solar thermal and photovoltaic potential on urban scale. Such areas require calculating accurately the specific shadow cast profile by nearby obstructions throughout each day and season.

A shadow cast model must address multiple requirements, as the accuracy of the results, the adaptability to the different building shapes and orientations and finally, the scalability. Although there are many algorithms to obtain shadow profiles in urban environments, there is still no methodology which fulfills simultaneously the three above-mentioned requirements. Therefore, the primary goal of the present study was to perform and validate a simple solution for shadow profile cast calculation achieving:

- A good accuracy by applying analytical vector-based models.
- An adaptable model based on robust statistical estimators and able to calculate cast shadows on arbitrary sloped and orientated surfaces.
- A scalable methodology starting from open and available data in most countries and integrating the model into widely used 2D-GIS environments.

Nowadays, the most common way to perform shading calculations is usually with design-oriented software. Design-oriented models of buildings can predict their shadows with great precision. This software includes specialized applications such as Radiance [10], TOWNSCOPE II [11] or SOLENE [12] and general 3D-CAD or BIM applications such as SketchUp [13], Rhinoceros [14] or Autodesk Revit [15]. Although design-oriented software has a high accuracy and provides advanced visualization capabilities, the high computational cost in the specialized software and the lack of availability of 3D-CAD data at large scale or a city level, the use of these tools is usually limited to a local or architectural scale [7,16]. In order to model and analyze entire cities, non-analytical approaches have also been proposed, such as Machine Learning [17,18], which is a computationally efficient alternative to analytical methods. However, those approaches cannot completely replace analytical models, especially in environments with complex geometries such as the urban landscape.

Among the analytical methods and for areas up to some square kilometers, shadow calculations and other spatial analysis are usually performed using Geographic Information Systems (GIS) models, which have proved to be the most powerful method to estimate the solar potential [8]. In these environments, shadow calculations have been commonly performed with a raster-based approach based on a digital elevation model (DEM) employing common open-source tools such as *r.sun* model [19] in GRASS GIS, the *doshade* command in the *insol* R package [20] or using proprietary software as the Solar Analyst extension [21] in ArcGIS. These tools have specific routines for the calculation of shadows using ray-tracing algorithms based on a DEM whereby the sunlight obstruction is evaluated for every grid cell for a given timestamp or solar position. This approach has the advantage of simplicity and high-speed processing, although this is at the expense of accuracy and large file size, both of which depend on the grid resolution [22]. Additionally, raster-based models are appropriate for modelling data changes continuously across a region, such as the natural terrain, where the grid resolution is not critical. Furthermore, raster models cannot be employed in areas of differing relief complexity nor for the modelling of vertical surfaces since they would present discontinuities.

Different strategies have been developed recently to assess the solar potential on vertical surfaces which significantly contribute to the overall solar potential of modern cities [23] due their high areas. These include models based on hyperpoints [24,25], 2D triangular mesh [26,27] and 3D-voxel [28,29]. The latter are all grid-based models that discretize the space in basic computational elements such as hyperpoints, triangles or voxels, and apply ray-tracing algorithms to the planar-mid-point of the element.

However, the previous approaches are usually not available or not implemented in common GIS software. Furthermore, only some of these publications [25,27] have validated the radiation results and none of them have experimentally validated the shadow results separately from the solar radiation.

The other type of data in common GIS environments is vector data. Vector data in GIS is formed by one or more interconnected vertices or points which generate spatial entities representing real-world features, such as buildings. The accuracy of this approach depends on scale and the desired level of detail [30]. Vector-based models are more appropriate to automatically model [31,32] and analyze fine-scale urban spaces, characterized by a highly variable and discontinuous relief, and common available data, such as LiDAR and building footprints datasets.

The degree of complexity of a 3D model in GIS environments is categorized according to the level of detail (LoD) concept of the standard CityGML [33]. Although there are many models

and strategies to obtain a vector-based 3D city models from LiDAR data, usually these methods are sensitive to the local point density as well as to the noise, outliers and missing data [34]. The higher the LoD the higher the density of required points. Furthermore, the use of high LoDs for analytic purposes increases substantially the computational cost or limits the scale of the model to be processed. In contrast, calculation errors due to the use of a low granularity (LoD) could be high [35]. Therefore, the LoD must be carefully selected according to the shape of the buildings, the accuracy and the extension of the study. Furthermore, the LoD should be coherent with the quality and availability of the LiDAR datasets.

Wang et al. [34] stated that the prismatic modelling (LoD1) is suitable for multilevel flat buildings which prevail in cities. In parallel, the open and available sources in most countries are usually low-density airborne LiDAR data (<1 pts/m^2) which are coherent with the different variants of LoD1 proposed by Biljecki et al. [36]. Then, the prismatic modelling, which is the simplest LoD, thoroughly models the real-world features in an urban context and can be applied to large areas using low computation resources.

Assuming a given fine footprint of the buildings (i.e. cadastral map), the critical parameter to model accurately in LoD1 is the building height which, as the geometric reference of the model, could have higher influence on the results than the granularity (LoD) of the model according to Biljecki et al. [35]. This is a key point particularly in shadow analysis, where an error in the geometric model may involve much larger errors in the shadow cast [37]. As a consequence and giving the considerable level of contamination of LiDAR datasets, statistical estimators with high robustness to outliers are essential to obtain correct height values of each building and therefore, to enable accurate shadow calculations.

Vector-based shadow algorithms are based on the search for the intersections between the sun rays and the surface of interest [38,39]. Recent publications contribute to their advance in GIS environments [29,40–43]. Among the previous literature, the shadow model used by Vulkan et al. [42] and implemented in the *shadow* R package [44], allows the calculation of shadow profiles on horizontal planes based on a 2.5D vector-based model through trigonometric relations. The present work tries to move a step beyond the previous shadow model of Vulkan et al. [42] by adding the possibility to calculate shadows on tilted surfaces, and by including a quantitative validation of the model.

This paper proposes and validates a simple solution for shadow modelling in cities from open and available data in most countries and using widely used 2D-GIS environments. Given the previous literature review, the present model includes the following novelties:

- Analytical vector-based shadow model to obtain a non-discretized shadow profile cast in arbitrary sloped and orientated surfaces integrated in the widely used 2D-GIS environment.
- Quantitative experimental validation of the shadow model for five-hour interval of two representative days in three surfaces of different slopes.
- Analysis and discussion on the best robust mode estimators to calculate the height of the buildings using LiDAR data.

2. Model description

The developed methodology is able to obtain a 3D vector-based city model of the existing buildings and their cast shadow profiles over any arbitrarily orientated and tilted planar surface in a 2D-GIS environment (scheme in Figure 1). The methodology consists in building a 3D city model (steps 1 to 3) in a 2D-GIS environment, using high robust statistic estimators. After this, an analytical shadow model is applied (steps 5 to 9) to calculate the shadow profile on any arbitrarily orientated and tilted 3D surface for any time of the year.

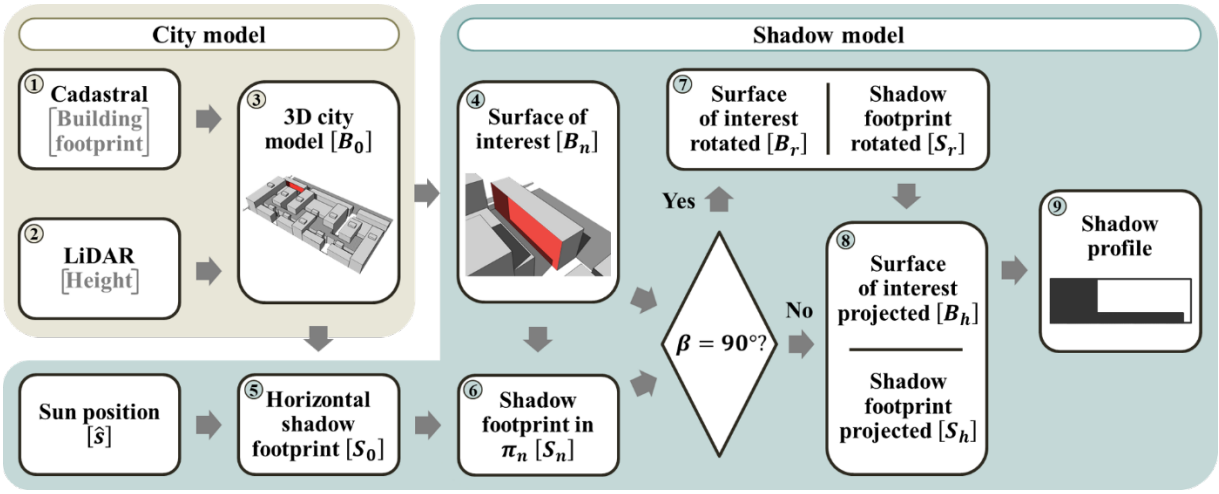

Figure 1. Workflow of the proposed methodology.

The modelling approach starts with the use of the cadastral map (1) and the contained LiDAR data (2) to build the 3D city model (3) by the vertical extruding of the buildings' footprint with their estimated height value. Once it has been obtained and given the sun position, the shadow model starts by calculating the horizontal shadow footprint (5). The latter, combined with the plane equations of the shaded surface (4), is projected onto the plane of the surface of interest surface of interest (6). Finally, depending on the slope $\boldsymbol{\beta}$ of the surface of interest the model processes differently these results in a 2D-GIS environment. In non-vertical surfaces (8), the shadow profile (9) is obtained as the intersection of the horizontal projection of the surface of interest and the shadow footprint, while in vertical surfaces (7) a previous rotation of the two polygons in the horizontal plane is required.

2.1 City model

First, a model of the desired buildings, district or city is developed. The starting point is the flat footprint of the buildings included in the cadastral cartography and the associated LiDAR point cloud dataset, which contains the height value Z of a XY regular grid.

A vector-based 3D model of the buildings is then obtained following a similar procedure to Ledoux and Meijers [45]. The latter is based on the vertical extruding of the 2D building footprint, with a height value Z obtained by a statistic estimator of the LiDAR points contained in each polygon.

These height values of each building can be assumed as a sample drawn from a unimodal, continuous distribution. Because of the nature of the data (e.g. presence of obstacles or clouds, planimetric and altimetric uncertainties or disparity between the footprints) these samples may contain a very significant presence of outliers or data from outside the population which is sampled. As a consequence, the height values of the LiDAR data enclosed within a building footprint are a potentially highly skewed and kurtotic sample [46]. For this reason, a proper measure of the central tendency, with low bias and high efficiency and robustness to outliers, is essential to obtain accurate and reliable information from these datasets.

In this paper, the seven high robust statistic estimators studied by Bickel [47] and Bickel and Frühwirth [48] have been considered to measure the central tendency. Furthermore, the arithmetic mean or central value, used in many cases in the generation of LiDAR-based city models [45,49], has been included in the comparative study. As indicated in the results, the latter has shown that the mean value is not a proper estimator of the building height due to its inherent outlier sensitivity. The robust statistics correspond to the median and the six mode estimators studied in Bickel and Frühwirth [48] which can be classified into three groups:

(1) Kernel density estimation: non-parametric method to estimate a smoothed empirical probability density function of a random variable. Considering a Gaussian kernel K, the

density function f of a random variable x based on a finite data sample $\{x\}_{i=1}^{n}$ is given in Eq.(1):

$$f(x) = \frac{1}{nh}\sum_{i=1}^{n} K\left(\frac{x - x_i}{h}\right) = \frac{1}{nh\sqrt{2\pi}}\sum_{i=1}^{n} \exp\left[-\frac{1}{2}\left(\frac{x - x_i}{h}\right)^2\right] \quad (1)$$

where $h > 0$ is the smoothing parameter called the bandwidth which balances the trade-off between bias and noise, hence the choice of h is crucial for the performance of its estimator. Then, the bandwidth selection is based on the optimal properties of f by using the Sheather & Jones (1991) procedure [50] implemented in the *stats* R package [51]. Once the function f is obtained, the empirical probability density function mode (EDFM) is defined as the value for which f reaches a maximum.

(2) Direct estimation: this set of methods does not involve density estimation. Four different mode estimators have been considered: the half-range mode (HRM) which is based on finding iteratively the half-range modal interval, defined as the interval of fixed range that contains the maximum number of observations. The half-sample mode (HSM) is also based on the iterative calculation of the modal interval, in this case using half-samples instead of half-ranges. Finally, the last two estimators are non-iterative and use only the first shortest half-sample to estimate the mode. These estimators are the shorth mode (SM), defined as the mean of these points, and the least median of squares mode (LMSM), defined as the midpoint.

(3) Parametric estimation: this estimation is based on the data transformation into a normal distribution and then on an analytical calculation of the mode of this transformed data. Within this group of procedures, the strategy proposed by Bickel [47] has been considered. In this case, a power transformation $y = x^{\lambda}$ with respect to the power parameter λ is applied and the mean μ and standard deviation σ of the transformed data y is estimated using the sample median and the standardized median absolute deviation. The robust parametric mode (RPM) can be estimated according to the Eq.(2):

$$\mathrm{RPM} = \left[\frac{1}{2}\left(\mu + \sqrt{\mu^2 + \frac{4\sigma^2(\lambda - 1)}{\lambda}}\right)\right]^{\frac{1}{\lambda}} \quad (2)$$

The previous statistical estimators have all been compared with CAD elevation views in order to determine which estimator is the best estimate for the actual building height. As a result, an LoD1 block model of the city is obtained according to the level of detail (LoD) concept of the standard CityGML [33], which indicates the complexity and the degree of abstraction of a 3D city model. This 3D city model, also known as 2.5D model, is easily integrated in 2D-GIS environments by saving the height value of each 2D building polygon as an attribute in the associated database.

2.2 Shadow model

The shadow model consists in an analytical procedure, applied and integrated in 2D-GIS environments, to obtain the shadow profile on any arbitrarily orientated and tilted surface for any point in time.

Once the buildings are defined, in order to implement the shadow model, a distinction is established between the shading objects (which cast shadows) and the shaded objects or surface of interest which receive such shadows.

The shading objects are fully defined by the 3D block city model. For the shaded objects, the associated database contains the centroid G height value of each polygon (Z), its inclination (β) and orientation (α) of the plane π_n.

The shadow profile is represented in a 2D-GIS environment given its projection S_h onto the horizontal plane π_h. The shadow factor SF is defined as the ratio of the shaded area S_n with respect to the total surface B_n. The shadow factor is consequently equal to the ratio of their horizontal projections, as indicated in Eq.(3):

$$SF = \frac{S_n}{B_n} = \frac{S_h}{B_h} \tag{3}$$

The shadow model starts from the shadow footprint S_0 on a horizontal plane π_h by means of the model developed by Vulkan et al. [42]. This model consists in shifting the contour of the buildings in the opposite direction to sun azimuth by a distance depending on the building height and the sun elevation.

Once the corresponding polygon S_0 is obtained, the model applies the operation of projection onto a plane along the direction of a given vector for each vertex p_0 of the polygon S_0. Specifically, the model calculates its projection S_n onto the plane π_n in the direction of the sun $\hat{s}$ by applying vector equations to each point p_0. The projected point p_n of point p_0 onto the plane π_n in the specified direction $\hat{s}$ is given in Eq.(4):

$$\begin{aligned} &p_n = p_0 - t \cdot \hat{s} && t = \frac{\hat{n} \cdot \overrightarrow{v_1}}{\hat{n} \cdot \hat{s}} && \overrightarrow{v_1} = G - p_0 \\ &p_0 \in \pi_h && p_n, G \in \pi_n && \|\hat{n}\| = \|\hat{s}\| = 1 \end{aligned} \tag{4}$$

Once the projection p_n of each vertex p_0 is obtained, the polygon S_n is assembled. In order to integrate the results in a 2D-GIS environment and to use the corresponding tools, the model distinguishes between vertical and non-vertical shadowed surfaces (Figure 2).

For non-vertical surfaces, the representation of the shadow profile in a 2D-GIS environment is obtained as the intersection between the horizontal projection of the surface of interest B_h, which is usually equivalent to the given footprint, and the shadow footprint S_h, obtained by projecting each vertex p_n of the polygon S_n on the horizontal plane π_h, i.e., setting the height of each vertex p_n to zero.

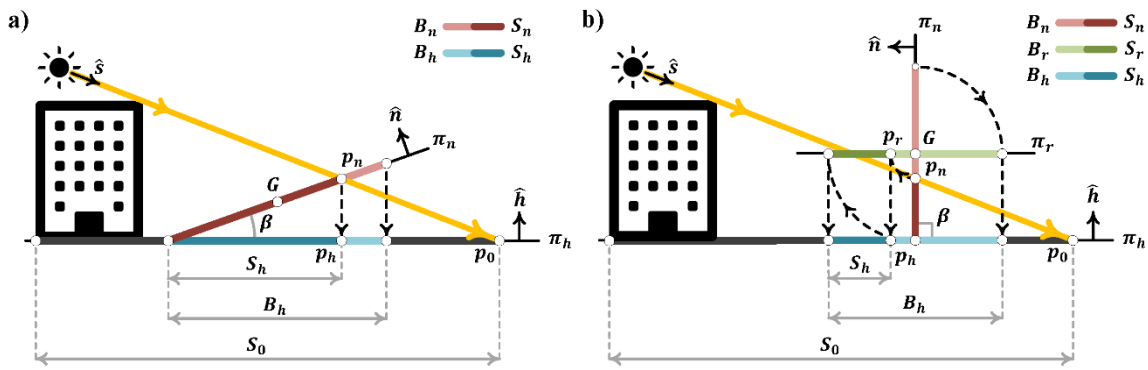

Figure 2. Shadow model for a) non-vertical and b) vertical surfaces

For vertical surfaces, it is not possible to apply the previous approach given that, on a horizontal 2D environment, the vertical surfaces are represented as lines and not as polygons.

For this reason, a rotation is applied to the surface of interest B_n and the shadow footprint S_n onto a plane π_r, which is not vertical. Thus, the rotated surface of interest B_r and the shadow footprint S_r is obtained using a same angle θ and rotation axis $\hat{u}$ for both polygons.

Although any non-vertical plane π_r could be considered, the horizontal plane at G point (π_r in Figure 2) is recommended, because in this way the real magnitude of the shadow profile is obtained. The angle θ and the axis of rotation for this operation is given in Eq.(5):

$$\theta = \text{acos}\frac{\hat{n}\cdot\hat{h}}{\|\hat{n}\|\cdot\|\hat{h}\|} \qquad \hat{u} = \frac{\hat{n}\times\hat{h}}{\|\hat{n}\times\hat{h}\|} \tag{5}$$

When the angle and axis has been considered, the resulting rotation of such polygons on a horizontal plane is achieved by applying the Rodrigues' rotation formula [52] to every vertex p_n of the polygons B_n and S_n. Eq.(6) defines the calculation, according to the right-hand rule, of the resulting rotated point p_r of point p_n by an angle θ, rotation axis $\hat{u}$ and using G as a center of rotation:

$$\begin{aligned} &p_r = G + \overrightarrow{v_2}\cdot cos\ \theta + (\overrightarrow{v_2}\cdot\hat{u})\cdot\hat{u}\cdot(1-cos\ \theta) + (\hat{u}\times\overrightarrow{v_2})\cdot sin\ \theta \\ &p_r \in \pi_r \qquad \overrightarrow{v_2} = p_n - G \qquad \|\hat{u}\| = 1 \end{aligned} \tag{6}$$

Once the non-vertical rotation p_r of each vertex p_n is obtained, the polygons S_r and B_r are assembled. Finally, the shadow profile in a 2D-GIS environment is obtained by applying the same procedure than for non-vertical shadowed surfaces, i.e., which is intersecting their horizontal projection.

3. Results, model validation and discussion

The methodology has been applied to several buildings of the Polytechnic City of Innovation (CPI) of the Universitat Politècnica de València (39°28’58’’N, 0°20’52’’O), which is located in the east of Spain (Figure 3). Such buildings present two significant points of interest for the validation which are that the detailed architectural CAD drawings from the construction are available, and that the buildings cast shadows on horizontal, vertical and tilted surfaces of the surroundings.

The methodology has been implemented in the R programming language [47] and has been validated using 3D-CAD software.

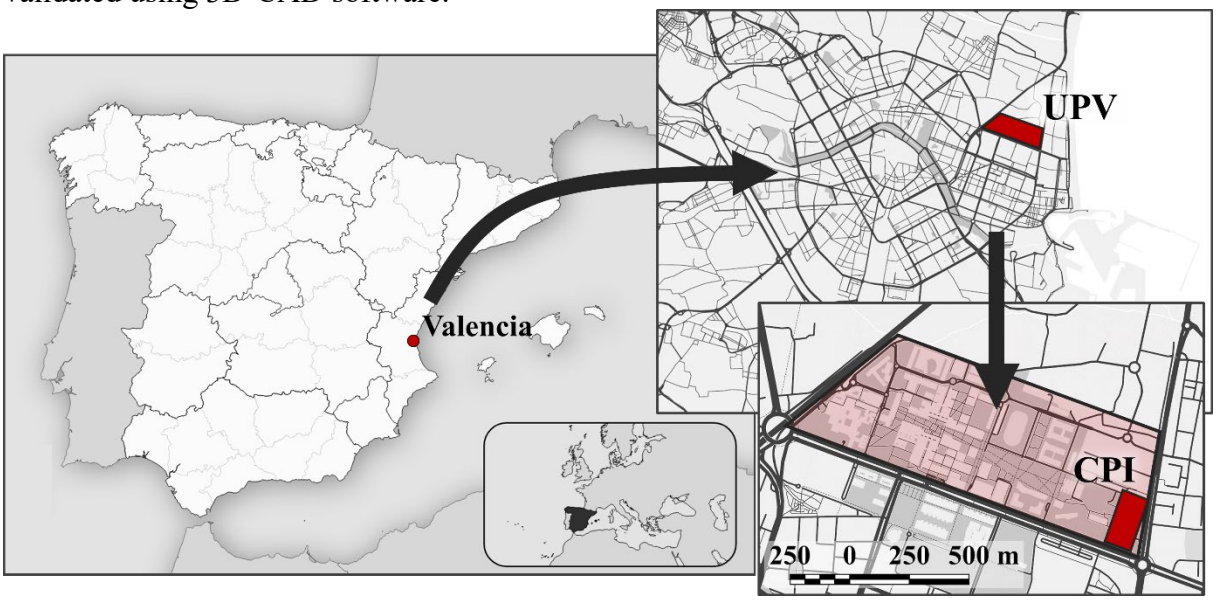

3.1 Figure 3. Location of the case study site in Valencia, Spain.City model

The CPI consists of 30 multilevel flat buildings. The total building footprint area is of around 12700m^2, placed in a 190x90m land, with building height values in the range from 14 to 29m with respect to the ground level, with a footprint area between 50 and 2150m^2. Along the west side of the CPI, there is a 6º tilted garden over 20m width, approximately.

In order to validate the city model, the height of each building was obtained using the statistic estimators of central tendency explained in the Section 2.1 compared to the mean, as evidence of their robustness towards outliers, and two open access government LiDAR datasets of low-density (0.5 pts/m²), which correspond to the years 2009 and 2015 [53].

The accuracy of each statistic applied to each dataset has been evaluated by comparing the results obtained with the heights defined in the CAD elevation views. Two error estimators have been calculated for each case: the root-mean-square error (RMSE) and the mean absolute error (MAE), as given in Eq.(7):

$$RMSE = \sqrt{\frac{\sum_i^n \left(x_{CAD,i} - x_{model,i}\right)^2}{n}} \qquad MAE = \frac{\sum_i^n \left|x_{CAD,i} - x_{model,i}\right|}{n} \tag{7}$$

Both error metrics are used together to measure the model performance. The MAE is used to evaluate the average magnitude of the error while the RMSE, compared with the prior, is employed to diagnose the presence of large errors. The RMSE and MAE of each estimator and LiDAR dataset for all the buildings has been obtained in meters. The results are shown in Table 1, where the final row "total" has been calculated by running estimators over the merged LiDAR datasets.

	RMSE (MAE) [m]							
	SM	**LMSM**	**HSM**	**HRM**	**EDFM**	**RPM**	**Median**	**Mean**
LiDAR 2009	0.061 (0.047)	0.060 (0.047)	0.064 (0.050)	0.063 (0.051)	0.063 (0.048)	0.065 (0.053)	0.065 (0.052)	1.423 (1.222)
LiDAR 2015	0.061 (0.045)	0.061 (0.045)	0.059 (0.045)	0.063 (0.049)	0.056 (0.043)	0.062 (0.046)	0.062 (0.046)	1.306 (1.073)
Total	0.061 (0.046)	0.061 (0.046)	0.061 (0.047)	0.063 (0.050)	0.060 (0.046)	0.064 (0.050)	0.063 (0.049)	1.366 (1.148)

Table 1. Root-mean-square error and mean absolute error of city models in two LiDAR datasets.

Very similar results can be observed for the seven high robust statistics studied by Bickel and Frühwirth [48]. These measures of central tendency show mean errors lower than 0.1m and no significant differences between the two datasets are observed. Such results are consistent with the employed LiDAR datasets, which present a maximum RMSE in the Z coordinate of 0.20m [53].

Despite the high level of similarity between the different statistical estimators, the estimator which provides the best fitting with the real height, according to the results of the most recent (2015) and the merged set of LiDAR data, is the empirical probability density function mode (EDFM) based on a Gaussian kernel function and using the bandwidth according to the Sheather and Jones [50] procedure.

In contrast, the mean value is not a proper estimator of the building height, since it presents a high error due to its high sensitivity to outliers.

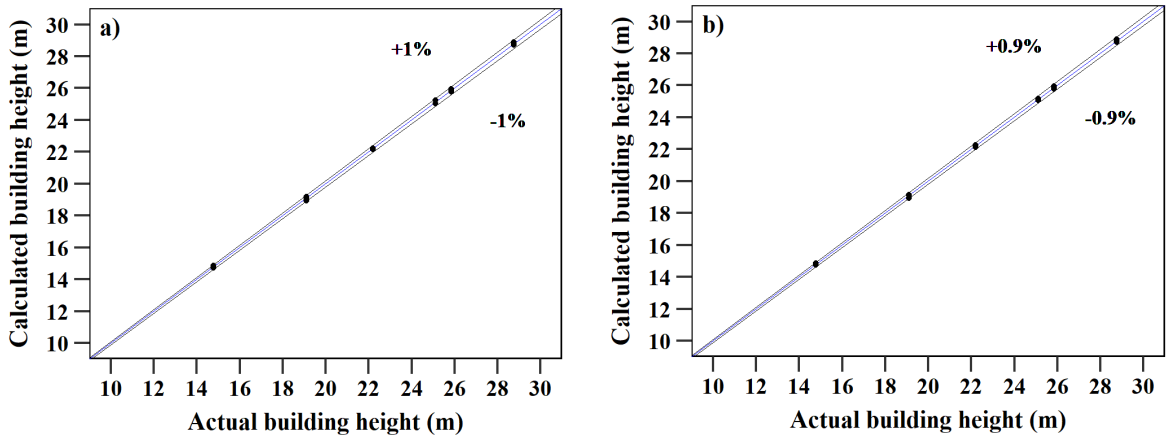

Figure 4. City model fit using the empirical probability density function mode (EDFM) for two LiDAR datasets: a) 2009 and b) 2015.

Figure 4 shows a comparison between the actual building height, extracted from the CAD drawings, and the height obtained by the proposed model, using the EDFM with both LiDAR datasets. The maximum relative error is smaller than 1% in all cases.

3.2 Shadow model

In order to apply and validate the shadow model, the best building height estimator and LiDAR dataset have been taken, which corresponds to the EDFM of 2015 data. For such model, the shadow profile has been calculated in three surfaces (Figure 5) with different β inclination (A-horizontal, B-vertical and C-tilted) for five hours (from 10 to 14 local time) at both solstices to test both short and long shadows for the location.

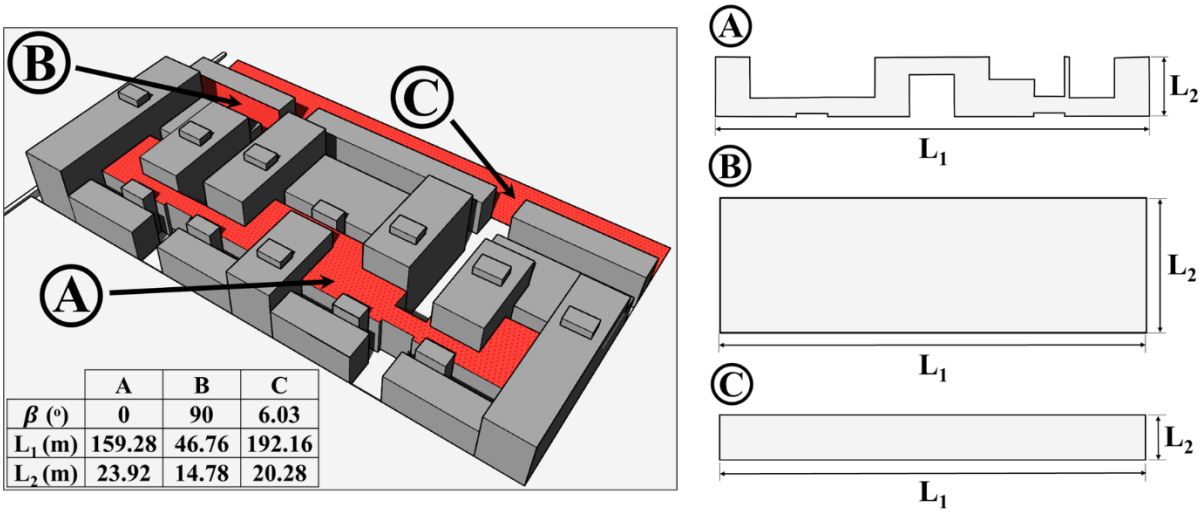

	A	B	C
β (°)	0	90	6.03
L_1 (m)	159.28	46.76	192.16
L_2 (m)	23.92	14.78	20.28

Figure 5. Studied surfaces of the Polytechnic City of Innovation (CPI): horizontal (A), vertical (B) and tilted (C).

In order to have a reference, the set of buildings has been modelled in SketchUp using their detailed architectural 2D-CAD views. The shadow profile has been obtained for each surface and hour (Figure 6) by using the SketchUp's shadow tool developed by Yezioro and Shaviv [54].

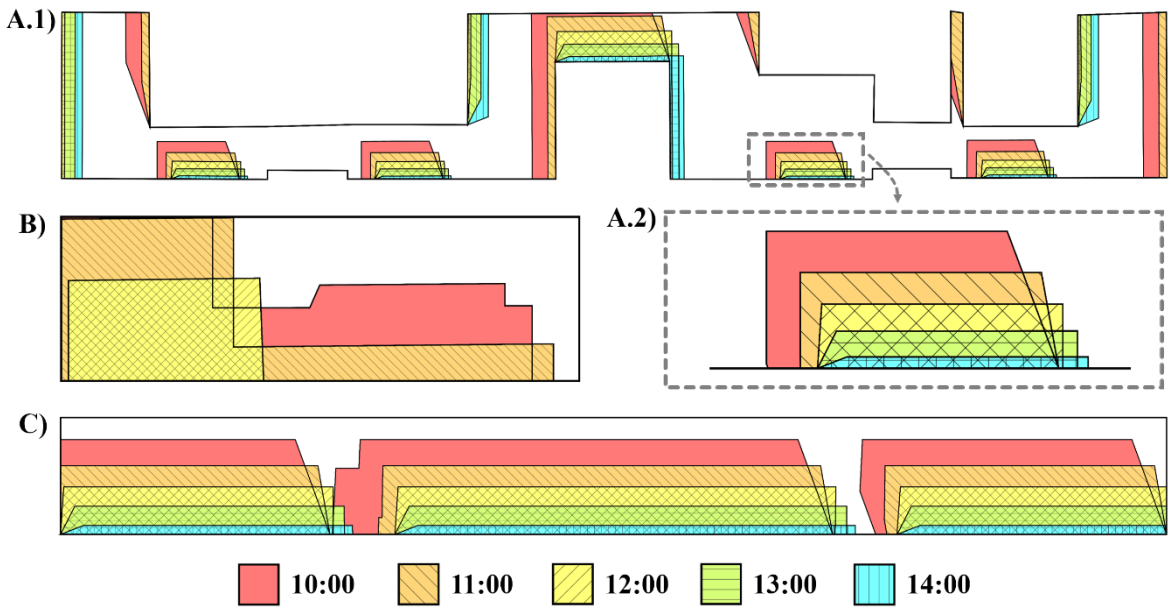

Figure 6. Shadow profiles on the studied surfaces for five hours on June 21st: horizontal surface (A.1) and its detail (A.2), vertical surface (B) and tilted surface (C).

Following the procedure explained in the Section 2.2, the shadow factor and the relative error series have been obtained for the five-hour interval of each representative day in the studied surfaces.

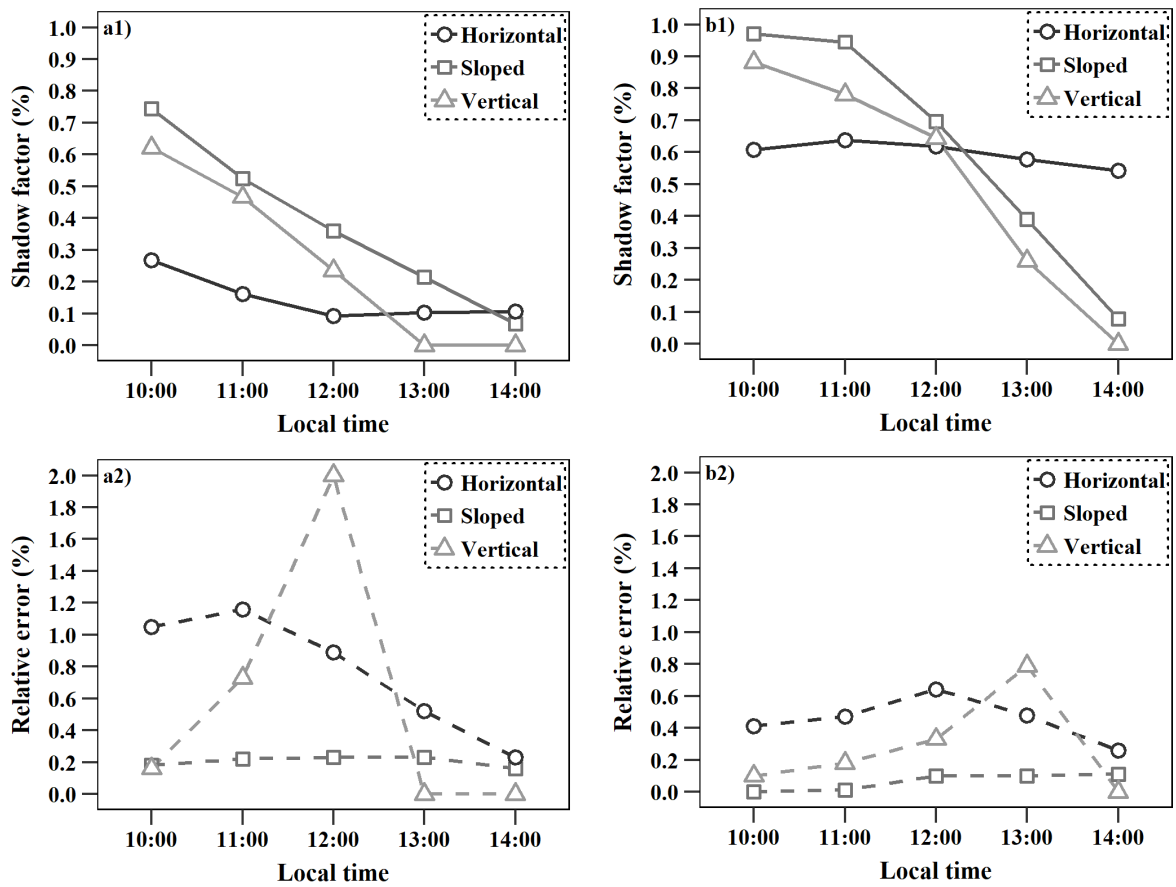

Figure 7. Hourly shadow factor (1) and their relative error (2) against the SketchUp's shadow tool results for a) the June 21st and b) December 22nd.

Figure 7 plots the shadow factor *SF* series and their relative error (RE) against the CAD (Sketchup) results as given in Eq.(8).

$$RE = \frac{|SF_{CAD} - SF_{model}|}{SF_{CAD}} \quad (8)$$

On the one hand, the time series of the shadow factor SF show that the shading is significantly greater in the early hours of the morning than in the early afternoon on the inclined and vertical surfaces, while for the horizontal surface the inter-daily fluctuations are not so variable.

These results are explained taking into account that the two non-horizontal surfaces are oriented to the southeast ($\alpha = 288.6°$, counterclockwise convention measuring from the south), so the shadows are null in this orientation at 14:26 local time for June 21st and 14:14 local time for December 22nd. There are taller buildings in the southeast and southwest direction, which explains the small variation of the shadow factor on the horizontal surface.

Regarding the annual variation of the shadow factor, the results show that the shading is much greater in the winter solstice than in the summer solstice, mainly because the solar elevation in winter is much lower in the site latitude.

On the other hand, the series of the relative error show higher accuracy on the sloped surface than on the horizontal, while for the vertical surface this precision is variable over time, showing maximums at certain time points. The two primary elements influencing the model accuracy are:

1. The city model error propagation, since the errors in the geometric model could lead to greater errors in the shadow cast. The height of the buildings that cast shadows on the sloped surface has an average error of 3cm, similar to the values of the other surfaces, which are 5cm for the horizontal and 6cm for the vertical surface. However, the shadow on the vertical surface presents the maximum relative error on June 21st at 12:00 local time when the shadow cast is only due to a building whose height error is 10cm.
2. The shadow and surface size, since the shadow factor SF is a relative measure of the shaded area with respect to the total surface area. For this reason, the accuracy is logically greater in larger areas.

Therefore, the greater precision of the model in the sloped surface is due to the combination of a greater precision in the city model and to a large area and shadow size (Figure 6).

However, despite these differences between the results obtained, the most notable aspect of the series of the relative error is the very low error which is obtained.

For the validation of the overall methodology, including both height and shadow models, the shadow profiles were also obtained in the SketchUp's shadow tool and the shadow factor SF was calculated in each case. Table 2 presents the RMSE and the MAE of the overall methodology by the shadow factor obtained against the SketchUp results of each surface and day.

	RMSE (MAE) [%]		
	June 21st	**December 22nd**	**Total**
Horizontal (A)	0.16 (0.13)	0.29 (0.27)	0.23 (0.20)
Vertical (B)	0.26 (0.18)	0.15 (0.13)	0.21 (0.16)
Sloped (C)	0.09 (0.08)	0.04 (0.03)	0.07 (0.05)
Total	0.18 (0.13)	0.19 (0.14)	0.19 (0.14)

Table 2. Root-mean-square error (RMSE) and mean absolute error (MAE) of the overall methodology measured by the shadow factor obtained against the SketchUp's shadow tool for different days and surfaces.

The results show that the average accuracy of the shadow factor on the sloped surface is significantly higher than in the other two surfaces according to the relative errors shown in Figure 7.

In contrast, the results show no significant differences between the total values of the two selected days. However, there are significant and complementary differences between the vertical and horizontal surface at both solstices, because the surfaces are perpendicularly oriented.

Finally, Figure 8 summarizes the validation of the overall methodology for the three surfaces on the two representative days. The hourly results of the model have been compared with respect to the reference SketchUp's shadow tool results.

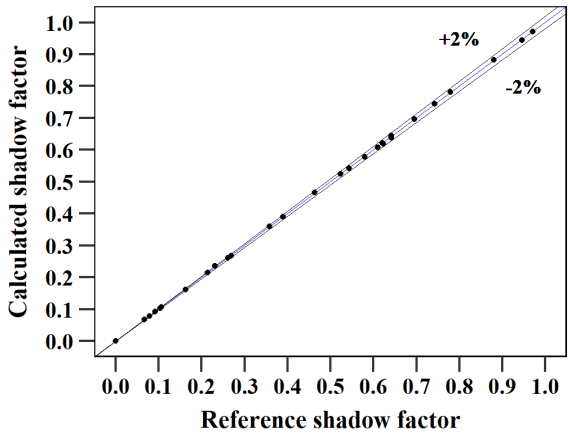

Figure 8. Overall methodology fit for all surfaces through the shadow factor evaluation.

4. Conclusions

An accurate estimation of shadow profiles is essential for several downstream applications on urban scale. In these applications, a shadow cast model must be accurate, adaptable to the geometric complexity of the buildings and scalable.

The present article presents an accurate and systematic GIS-based methodology which has been developed to obtain the shadow cast by a group of buildings on arbitrarily orientated and tilted surfaces. The methodology is integrated into the scalable and widely used 2D-GIS environment and can be useful for the solar resource assessment in fine-scale urban environments of most countries using open access data.

The starting point of the model is to employ cadastral cartography and LiDAR altimetric data to obtain a 3D vector-based model of the existing buildings, by means of robust statistical estimators. Analytical models are finally applied for the calculation of the shadow cast on any surrounding surface.

The above-mentioned methodology has been validated on 30 buildings of the Universitat Politècnica de València (UPV, Spain). The validation has been performed using the CAD elevation views of the buildings and 3D-CAD software. Different LiDAR point cloud datasets have been employed and evaluated for the 3D model validation, while the shadow model has been validated for both different surface orientations and points in time. The following conclusions have been drawn:

- The error obtained in the validation of the vector-based 3D model of the buildings is lower than 1% with all robust mode estimators.
- The mean value is not a proper estimator of the building height because of its inherent high sensitivity to outliers. The authors recommend to use robust estimators such as the EDFM.

- The maximum relative error of the overall methodology, including both 3D and shadow model, is lower than 2% for the shadow factor calculations.
- The accuracy of the model is not dependent on the day of the year or hour of the day but the shadow factor calculation is particularly sensitive to propagation of the height model errors of the involved buildings and, to a lesser degree, to the size of the shadow and the surface.

As future work, the presented methodology will be used to calculate the direct solar irradiation in buildings, including facades and tilted roofs. For a full solar resource assessment, the diffuse component will be considered by using the sky view factor (SVF) of the surfaces of interest. The methodology will be further improved by including a 3D city model that estimates the inclination and orientation of building roofs and a shadow model that uses them as shading objects.

Acknowledgements

This work has been supported by the Generalitat Valenciana inside the program "Subvencions per a la contractació de personal investigador de caràcter predoctoral (ACIF/2019/239)".

Declaration of interest

None

Bibliography

[1] U. Nations, D. of Economic, S. Affairs, P. Division, World Urbanization Prospects: The 2018 Revision, New York, 2019. https://doi.org/10.18356/b9e995fe-en.

[2] Coalition for Urban Transitions, Climate Emergency, Urban Opportunity, London and Washington, DC, 2019. https://urbantransitions.global/urban-opportunity/.

[3] R. Billen, A.-F. Cutting-Decelle, O. Marina, J.-P. de Almeida, C. M., G. Falquet, T. Leduc, C. Métral, G. Moreau, J. Perret, G. Rabin, R. San Jose, I. Yatskiv, S. Zlatanova, 3D City Models and urban information: Current issues and perspectives, in: EDP Sciences, 2014: pp. I–118. https://doi.org/10.1051/tu0801/201400001.

[4] F. Biljecki, J. Stoter, H. Ledoux, S. Zlatanova, A. Çöltekin, Applications of 3D city models: State of the art review, ISPRS International Journal of Geo-Information. 4 (2015) 2842–2889. https://doi.org/10.3390/ijgi4042842.

[5] C.F. Reinhart, C. Cerezo Davila, Urban building energy modeling - A review of a nascent field, Building and Environment. 97 (2016) 196–202. https://doi.org/10.1016/j.buildenv.2015.12.001.

[6] X. Oregi, N. Hermoso, I. Prieto, J.L. Izkara, L. Mabe, P. Sismanidis, Automatised and georeferenced energy assessment of an Antwerp district based on cadastral data, Energy and Buildings. 173 (2018) 176–194. https://doi.org/10.1016/j.enbuild.2018.05.018.

[7] S. Freitas, C. Catita, P. Redweik, M.C. Brito, Modelling solar potential in the urban environment: State-of-the-art review, Renewable and Sustainable Energy Reviews. 41 (2015) 915–931. https://doi.org/10.1016/j.rser.2014.08.060.

[8] R. Machete, A.P. Falcão, M.G. Gomes, A. Moret Rodrigues, The use of 3D GIS to analyse the influence of urban context on buildings' solar energy potential, Energy and Buildings. 177 (2018) 290–302. https://doi.org/10.1016/j.enbuild.2018.07.064.

[9] I. Lima, V. Scalco, R. Lamberts, Estimating the impact of urban densification on high-rise office building cooling loads in a hot and humid climate, Energy and Buildings. 182 (2019) 30–44. https://doi.org/10.1016/j.enbuild.2018.10.019.

[10] G. and S.R. Ward, Rendering with Radiance: The Art and Science of Lighting Visualization, Morgan Kaufman. (1998).

[11] J. Teller, S. Azar, Townscope II - A computer systems to support solar access decision-making, Solar Energy. 70 (2001) 187–200. https://doi.org/10.1016/S0038-092X(00)00097-9.

[12] F. Miguet, D. Groleau, A daylight simulation tool for urban and architectural spaces-application

to transmitted direct and diffuse light through glazing, Building and Environment. 37 (2002) 833–843. https://doi.org/10.1016/S0360-1323(02)00049-5.
[13] Trimble Inc., SketchUp, (2019). https://www.sketchup.com.
[14] Robert McNeel & Associates, Rhinoceros, (2019). https://www.rhino3d.com.
[15] Autodesk Inc., Autodesk Revit, (2020). https://www.autodesk.com/products/revit/overview.
[16] G. Desthieux, C. Carneiro, R. Camponovo, P. Ineichen, E. Morello, A. Boulmier, N. Abdennadher, S. Dervey, C. Ellert, Solar Energy Potential Assessment on Rooftops and Facades in Large Built Environments Based on LiDAR Data, Image Processing, and Cloud Computing. Methodological Background, Application, and Validation in Geneva (Solar Cadaster), Frontiers in Built Environment. 4 (2018) 14. https://doi.org/10.3389/fbuil.2018.00014.
[17] A. Vartholomaios, A machine learning approach to modelling solar irradiation of urban and terrain 3D models, Computers, Environment and Urban Systems. 78 (2019) 101387. https://doi.org/10.1016/j.compenvurbsys.2019.101387.
[18] D. Assouline, N. Mohajeri, J.L. Scartezzini, Quantifying rooftop photovoltaic solar energy potential: A machine learning approach, Solar Energy. 141 (2017) 278–296. https://doi.org/10.1016/j.solener.2016.11.045.
[19] J. Hofierka, M. Súri, The solar radiation model for Open source GIS: implementation and applications, in: Open Source GIS - GRASS Users Conference, 2002.
[20] J.G. Corripio, insol: Solar Radiation. R package version 1.2.1, (2019). https://cran.r-project.org/package=insol (accessed January 9, 2020).
[21] P. Fu, P.M. Rich, Design and Implementation of the Solar Analyst: an ArcView Extension for Modeling Solar Radiation at Landscape Scales, 19th Annual ESRI User Conference. (1999) 1–24.
[22] Esri, What is raster data? - Help | ArcGIS Desktop, (n.d.). https://desktop.arcgis.com/en/arcmap/latest/manage-data/raster-and-images/what-is-raster-data.htm (accessed January 9, 2020).
[23] M.C. Brito, S. Freitas, S. Guimarães, C. Catita, P. Redweik, The importance of facades for the solar PV potential of a Mediterranean city using LiDAR data, Renewable Energy. 111 (2017) 85–94. https://doi.org/10.1016/J.RENENE.2017.03.085.
[24] C. Catita, P. Redweik, J. Pereira, M.C. Brito, Extending solar potential analysis in buildings to vertical facades, Computers and Geosciences. 66 (2014) 1–12. https://doi.org/10.1016/j.cageo.2014.01.002.
[25] M.C. Brito, P. Redweik, C. Catita, S. Freitas, M. Santos, 3D Solar Potential in the Urban Environment: A Case Study in Lisbon, Energies. 12 (2019) 3457. https://doi.org/10.3390/en12183457.
[26] S. Kaynak, B. Kaynak, A. Özmen, A software tool development study for solar energy potential analysis, Energy and Buildings. 162 (2018) 134–143. https://doi.org/10.1016/J.ENBUILD.2017.12.033.
[27] J. Liang, J. Gong, J. Zhou, A.N. Ibrahim, M. Li, An open-source 3D solar radiation model integrated with a 3D Geographic Information System, Environmental Modelling and Software. 64 (2015) 94–101. https://doi.org/10.1016/j.envsoft.2014.11.019.
[28] J. Liang, J. Gong, A Sparse Voxel Octree-Based Framework for Computing Solar Radiation Using 3D City Models, ISPRS International Journal of Geo-Information. 6 (2017) 106. https://doi.org/10.3390/ijgi6040106.
[29] J. Hofierka, M. Zlocha, A New 3-D Solar Radiation Model for 3-D City Models, Transactions in GIS. 16 (2012) 681–690. https://doi.org/10.1111/j.1467-9671.2012.01337.x.
[30] QGIS Development Team, Vector Data - Documentation for QGIS 3.4, (n.d.). https://docs.qgis.org/3.4/en/docs/gentle_gis_introduction/vector_data.html (accessed January 9, 2020).
[31] Q.Y. Zhou, U. Neumann, Fast and extensible building modeling from airborne LiDAR data, in: GIS: Proceedings of the ACM International Symposium on Advances in Geographic Information Systems, 2008: pp. 43–50. https://doi.org/10.1145/1463434.1463444.
[32] J. Yan, K. Zhang, C. Zhang, S.C. Chen, G. Narasimhan, Automatic construction of 3-D building model from airborne LIDAR data through 2-D snake algorithm, IEEE Transactions on Geoscience and Remote Sensing. 53 (2015) 3–14. https://doi.org/10.1109/TGRS.2014.2312393.
[33] G. Gröger, L. Plümer, CityGML - Interoperable semantic 3D city models, ISPRS Journal of

Photogrammetry and Remote Sensing. 71 (2012) 12–33. https://doi.org/10.1016/j.isprsjprs.2012.04.004.
[34] R. Wang, J. Peethambaran, D. Chen, LiDAR Point Clouds to 3-D Urban Models : A Review, IEEE Journal of Selected Topics in Applied Earth Observations and Remote Sensing. 11 (2018) 606–627. https://doi.org/10.1109/JSTARS.2017.2781132.
[35] F. Biljecki, H. Ledoux, J. Stoter, G. Vosselman, The variants of an LOD of a 3D building model and their influence on spatial analyses, ISPRS Journal of Photogrammetry and Remote Sensing. 116 (2016) 42–54. https://doi.org/10.1016/j.isprsjprs.2016.03.003.
[36] F. Biljecki, H. Ledoux, J. Stoter, An improved LOD specification for 3D building models, Computers, Environment and Urban Systems. 59 (2016) 25–37. https://doi.org/10.1016/j.compenvurbsys.2016.04.005.
[37] F. Biljecki, G.B.M. Heuvelink, H. Ledoux, J. Stoter, Propagation of positional error in 3D GIS: estimation of the solar irradiation of building roofs, International Journal of Geographical Information Science. 29 (2015) 2269–2294. https://doi.org/10.1080/13658816.2015.1073292.
[38] W. Newman, I.E. Sutherland, G.W. Hodgman, Graphics and Reentrant Polygon Clipping, 1974.
[39] K. Weiler, P. Atherton, Hidden surface removal using polygon area sorting, ACM SIGGRAPH Computer Graphics. 11 (1977) 214–222. https://doi.org/10.1145/965141.563896.
[40] A. Strzalka, N. Alam, E. Duminil, V. Coors, U. Eicker, Large scale integration of photovoltaics in cities, Applied Energy. 93 (2012) 413–421. https://doi.org/10.1016/j.apenergy.2011.12.033.
[41] M. Weisthal, Assessment of potential energy savings in Israel through climate-aware residential building design, Ben Gurion University of the Negev, 2014.
[42] A. Vulkan, I. Kloog, M. Dorman, E. Erell, Modeling the potential for PV installation in residential buildings in dense urban areas, Energy and Buildings. 169 (2018) 97–109. https://doi.org/10.1016/j.enbuild.2018.03.052.
[43] S. Pili, G. Desogus, D. Melis, A GIS tool for the calculation of solar irradiation on buildings at the urban scale, based on Italian standards, Energy and Buildings. 158 (2018) 629–646. https://doi.org/10.1016/j.enbuild.2017.10.027.
[44] M. Dorman, E. Erell, A. Vulkan, I. Kloog, shadow: R Package for Geometric Shadow Calculations in an Urban Environment, The R Journal. 11 (2019) 287. https://doi.org/10.32614/rj-2019-024.
[45] H. Ledoux, M. Meijers, Topologically consistent 3D city models obtained by extrusion, International Journal of Geographical Information Science. 25 (2011) 557–574. https://doi.org/10.1080/13658811003623277.
[46] M. Bartels, H. Wei, D.C. Mason, DTM generation from LIDAR data using skewness balancing, in: Proceedings - International Conference on Pattern Recognition, 2006: pp. 566–569. https://doi.org/10.1109/ICPR.2006.463.
[47] D.R. Bickel, Robust and efficient estimation of the mode of continuous data: the mode as a viable measure of central tendency, Journal of Statistical Computation and Simulation. 73 (2003) 899–912. https://doi.org/10.1080/0094965031000097809.
[48] D.R. Bickel, R. Frühwirth, On a fast, robust estimator of the mode: Comparisons to other robust estimators with applications, Computational Statistics & Data Analysis. 50 (2006) 3500–3530. https://doi.org/10.1016/j.csda.2005.07.011.
[49] Esri, Obtaining elevation information for building footprints - Help | ArcGIS Desktop, (n.d.). https://desktop.arcgis.com/en/arcmap/latest/extensions/3d-analyst/3d-buildings-obtaining-elevation-information-for-building-footprints.htm (accessed January 9, 2020).
[50] S.J. Sheather, M.C. Jones, A Reliable Data-Based Bandwidth Selection Method for Kernel Density Estimation, Journal of the Royal Statistical Society. Series B (Methodological). 53 (1991) 683–690. http://www.jstor.org/stable/2345597.
[51] R Core Team, R: A Language and Environment for Statistical Computing, (2019). https://www.r-project.org/.
[52] H. Cheng, K.C. Gupta, An historical note on finite rotations, Journal of Applied Mechanics, Transactions ASME. 56 (1989) 139–145. https://doi.org/10.1115/1.3176034.
[53] Instituto Geográfico Nacional, Plan Nacional de Ortofotografía Aérea - Especificaciones técnicas, (n.d.). https://pnoa.ign.es/especificaciones-tecnicas (accessed January 9, 2020).
[54] A. Yezioro, E. Shaviv, Shading: A design tool for analyzing mutual shading between buildings, Solar Energy. 52 (1994) 27–37. https://doi.org/10.1016/0038-092X(94)90078-G.